First-principles molecular-dynamics study of glassy As_2Se_3

Jun Li and D. A. Drabold
Department of Physics and Astronomy, Condensed Matter and Surface Science Program, Ohio University, Athens, Ohio 45701-2979
(Received 3 November 1999)

A first-principles molecular-dynamics study of glassy As_2Se_3, using a 215-atom model, is presented. Our model is in good and uniform agreement with available measurements of the structural, vibrational, and electronic properties. The model reproduces the structure of the experimental static structure factor in the range $\sim 2-6$ Å^{-1}. The preferred structural unit is pyramidal $AsSe_3$ loosely coupled by Se. The model mean coordination number is 2.4. The vibrational density of states has two distinct bands. The broadband in the lower-energy range, up to about 20 meV, is dominated by modes extending widely over the network. The localized modes occur at the edges of the bands. The electronic density of states has also two main bands in the valence range. One is from the $4s$ electrons of As and Se; the other from $4p$ electrons populates on the upper energy range of the valence band. The calculated fundamental gap is 1.42 eV and the band tail states are localized predominantly on the coordination defects of As.

I. INTRODUCTION

Arsenic triselenide (As_2Se_3) has been extensively studied as a classic glass former for 30 years. A basic interest in this system arises from its average coordination number (2.4), which is at a threshold predicted by the theory of Phillips[1] and Thorpe.[2] At $\langle r\rangle = 2.4$ a dynamical transition is expected to occur [for $\langle r\rangle < 2.4$ floppy modes (very-low-energy harmonic lattice excitations) are anticipated from a Maxwell counting argument[2]]. This transition implies a fundamental relation between the topology of the network and the low-energy dynamical and thermal properties of glasses and glass forming ability.[1] In chalcogenide materials there is also a strong interaction between the vibrational modes and the electronic excitation (electron-phonon coupling), giving rise to important light-induced effects. Experimentally Hisakuni and Tanaka[3] found the mechanism of photoinduced fluidity in chalcogenide glasses including As_2Se_3 to be photoelectronic. Photomelting is also observed at low temperature in selenium,[4] but the detailed mechanism is still uncertain.[5]

As_2Se_3 displays an interesting character in the short-range environment. A similar bonding character of As_2Se_3 exists in the crystalline, glassy,[6] and even the liquid states[7] from an analysis of radial distribution functions (RDFs) from scattering experiments. However, the precise nature of the local environment around the As and Se atoms in glassy As_2Se_3(g-As_2Se_3) is difficult to infer from scattering experiments, because these elements have similar scattering attributes for x rays, neutrons, and electrons. There are two structural units proposed for g-As_2Se_3. One is based on the cluster model[8] consisting mostly of pyramidal $AsSe_3$ molecules,[9] and the other is the layer structure as in crystalline As_2Se_3 (c-As_2Se_3).[10,11]

At intermediate length scale the key structural signature is the first sharp diffraction peak (FSDP) near ~ 1.3 Å^{-1}. Neufville, Moss, and Ovshinsky[12] associated the FSDP with the molecular As_4Se_6 unit in films. Other authors[13,14] preferred correlation in the layer model of g-As_2Se_3. However, from a comparison of the RDF of c-As_2Se_3 with g-As_2Se_3 Renninger and Averbach[6] suggested that the layers must be distorted in g-As_2Se_3.

Many experimental efforts have been made on probing the possible types of bonds in networks of g-As_2Se_3 based on Raman and infrared spectra,[15] which measure the dynamical response of g-As_2Se_3. Lucovsky and Martin[16] calculated the optic mode frequencies of g-As_2Se_3 using a molecular model and several vibrational frequencies were assigned to pyramidal $AsSe_3$. A contribution from the bridging chain of Se has also been proposed.[17] A general vibrational character has been advanced to account for the composition independence of the lower-energy modes, the ''vibrational isocoordinate rule'' (VIR).[18,19]

There is also a controversy over the electronic structure from previous calculations on As_2Se_3. Chen[20] calculated the electronic structure of pyramidal $AsSe_3$ molecules in the layer configuration using molecular orbital methods. He found that the lone-pair states of Se lie below the bonding states. From his energy-level scheme he attributed the observed photodissociation and photocrystallization of g-As_2Se_3 to the breaking of the σ bonds by photons of band-gap energies. However, Kastner[21] pointed out that in chalcogenide materials the nonbonding p states of Se form a lone-pair band lying in energy between the σ bonding states and the σ^* anti bonding states. Both the σ and lone-pair bands are occupied and the σ^* band is unoccupied. This leads to a different picture of the properties of states near edges. Experiments on trigonal Se (Ref. 22) and recent theory work[23] gave a preference to Kastner's picture.

To our knowledge there is little theoretical work on the structure, vibrational, and the electronic structure of g-As_2Se_3 *all within one realistic model*. We felt the need for a model that simultaneously agreed with as many experiments as possible. This paper reports a first-principles-type molecular-dynamics (MD) study of g-As_2Se_3, using a 215-atom model. Our calculation gives a uniform agreement with the experiment on the structure, vibrational, and electronic properties of g-As_2Se_3. The *experimental* credibility of these models recommends them as a good starting point to investigate other phenomena such as light-induced effects.

II. MODEL GENERATION

The approximate first-principles-type MD program, FIREBALL96,[24] was used throughout this paper. In this calcu-

lation the Harris functional within the local density approximation was used in a scheme with the mathematical structure of nonorthogonal tight binding[25] and the use of no free parameters in constructing the Hamiltonian matrix. This method has achieved encouraging successes in a wide of amorphous systems: a-C,[26] a-Si,[27] a-Se,[23] a-$GeSe_2$,[28] and a-GaN.[29] This scheme does very well at producing experimentally credible models because of its nearly unique balance of accuracy and efficiency. In particular, experimentally realistic models require large supercell models and long time evolutions in addition to a suitable level of accuracy, which the present prescription offers.

It is important to have the MD simulation start from a suitable starting structure including the basic chemical order of the glass. Thus as an initial configuration of our model we cut out a cubic supercell, consisting of 86 arsenic atoms and 129 selenium atoms, with the side length of 18.50 Å, from the c-As_2Se_3.[30] This gave the correct stoichiometry and a density close to the evaporated films 4.31 g/cm^3.[12] This procedure ensures reasonable chemical order from the beginning. The initial cell lost its low crystalline symmetry belonging to the monoclinic system which cannot comply with the cubic symmetry. We let the cubic cell freely evolve 1 ps; during this process the crystalline layer structure was destroyed and the temperature grew rapidly to more than 2000 K. Then we equilibrated the cell to 2000 K over 1 ps. We take three steps to cool down the model. First, the cell was equilibrated at 1000 K for 1 ps; then we cooled it at 300 K over 1 ps. Finally the cell was steepest descent quenched to 0 K. All the calculation was done at constant volume using the Γ point to sample the Brillouin zone. Considering the large supercell it is reasonable to use the Γ point only.

III. STRUCTURAL PROPERTIES

The interference function $F(Q)$ gives a direct comparison with the experiments[6] and static structure factor $S(Q)$ has a mathematical form convenient to analyze. Both functions are used in this paper to exploit their respective advantages. The radial distribution function or the pair correlation function $G(r)$ provides some limited real-space information about the topology of the model. The coordination, bond distributions, and the basic molecular building blocks of the network are given by analysis of the local arrangement of atoms within the first shell range of $G(r)$. The intermediate range-order (IRO) is discussed with the ring statistics.

A. Interference function

The interference function $F(Q)$ is given by

$$F(Q)=\int_0^\infty G(r)\sin Qr\,dr,$$

where $Q=4\pi\sin\theta/\lambda$, $G(r)=4\pi r[\rho(r)-\rho_0]$, and ρ_0 is the average density, $\rho(r)$ the density function for pairs separated by r. The numerical tables of the x-ray scattering factors of Doyle and Turner[31] show that the relative difference of scattering amplitudes of As and Se is almost independent of Q in a wide range. It is therefore reasonable to assume the Q independence in the above formula.[6] In our calculation it is also assumed that As and Se have the same atomic scattering amplitude [we have checked this in detail and find only a tiny difference in $F(Q)$]. The pair density $\rho(r)$ reduces to $\rho(r)=(1/N)\Sigma_{i\neq j}^{r\leqslant R_c}\delta(r-r_{ij})$, where N is the total number of atoms in model and r_{ij} the separation between atom i and j. The integration to infinity was truncated at R_c so that no more than half of the side length of the supercell is included.

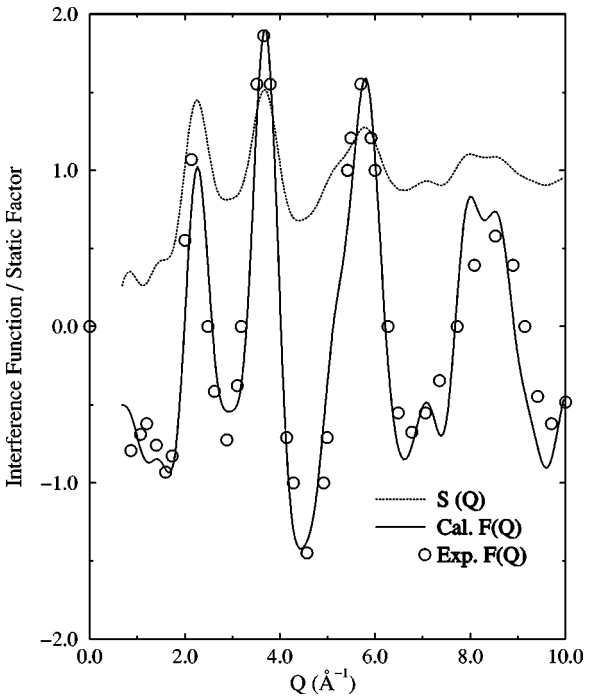

FIG. 1. Calculated and experimental (Ref. 6) interference function $F(Q)$ and static factors $S(Q)$ for g-As_2Se_3.

The calculated and experimental $F(Q)$ are compared in Fig. 1. The first three peaks agree closely with experiment[6] in the middle range ~ 2–6 Å^{-1}. The general trend for $Q<2$ Å^{-1} and $Q>6$ Å^{-1} still complies with observation though the detailed structure departs from the experimental data.

The static structure factor $S(Q)$ is related to $F(Q)$ as $S(Q)=1+F(Q)/Q$. One can expect that $S(Q)$ has the same peak structure as $F(Q)$ as shown in Fig. 1. From the calculation it is found that the third peak and features at higher Q depend mainly on the local environment. Once the nearest-neighbor atoms are taken into account the position of the third peak becomes fixed. To reproduce the second peak of $S(Q)$ [or $F(Q)$] R_c must be as large as 4.5 Å, corresponding to the whole second-nearest-neighbor shell in the radial distribution function $G(r)$. The position of the first peak at 2.43 Å^{-1} almost agrees with experiments as soon as the radial shell is enlarged to cover the third-nearest neighbor. This indicates that the first peak is a result of pair correlation at least on the scale of 6.5 Å. From the trend of agreement one can infer that the FSDP near 1.3 Å^{-1} requires a pair correlation of longer range.

We decompose $S(Q)$ to look for the contribution from different terms. The partial static factors are simply calculated as

$$S_{\alpha\beta}=\frac{1}{N}\sum_{\alpha\beta}^{r_{\alpha\beta}\leqslant R_c} j_0(Qr_{\alpha\beta}).$$

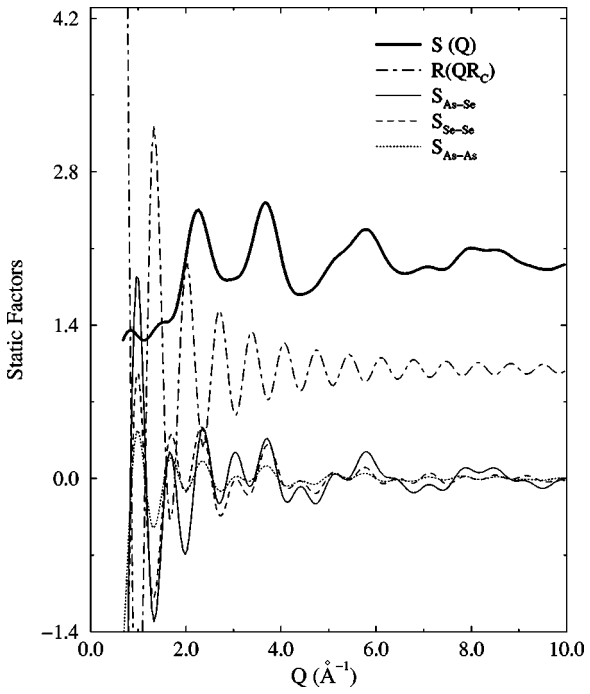

FIG. 2. Static factors $S(Q)$, remnant term $R(QR_c)$, and partial static factors $S_{\alpha\beta}$ for g-As_2Se_3. $S(Q)$ and $R(QR_c)$ are shifted up.

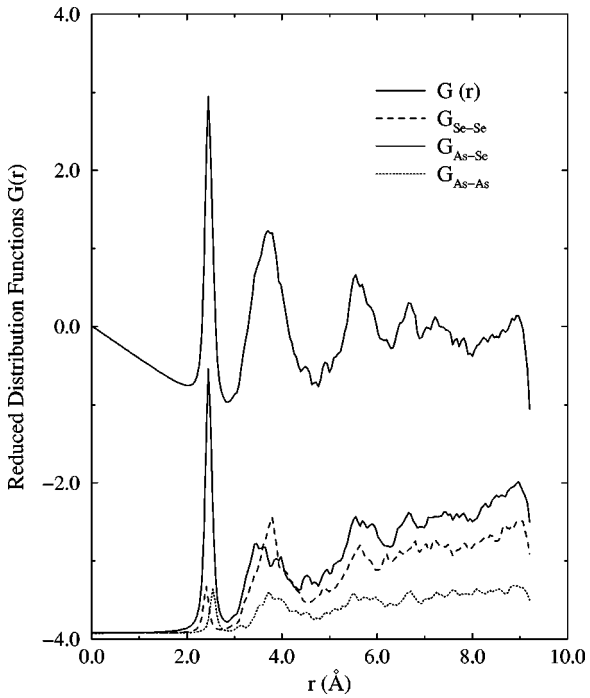

FIG. 3. Reduced atomic radial distribution and partial distribution functions for g-As_2Se_3.

The average density gives a remainder term $R(QR_c) = (3N_c/QR_c)j_1(QR_c)$ and $N_c = (4\pi R_c^3/3)\rho_0$. The j_0 and j_1 are spherical Bessel functions of the first kind. The total $S(Q)$ then is $1+\Sigma S_{\alpha\beta}+R(QR_c)$. The main components of $S(Q)$ are plotted in Fig. 2. The most interesting observation is the fast oscillation of the partial $S_{\alpha\beta}$ and the remainder $R(QR_c)$ but a slow oscillation in the total $S(Q)$. The cancellation between $S_{\alpha\beta}$ and $R(QR_c)$ gives a rather accurate and relatively smooth $S(Q)$. From $S_{\alpha\beta}$ it is clear that the correlation between As-Se pairs gives the main contribution to all the three dominant peaks of $S(Q)$, and Se-Se correlation gives a relatively strong contribution to the first two peaks, while As-As gives only a marginal contribution to the static factors. Because of the peaks at the lower-Q range, As-Se and Se-Se pairs are expected to have a correlation in a relatively longer range than As-As.

B. Short-range order

The reduced distribution function or pair correlation function $G(r)$ is given in Fig. 3. We associate each peak of $G(r)$ to a certain shell occupied by atoms in the radial distribution. The first shell is well defined; other shells have an increasingly ambiguous meaning as the properties of such shells are increasingly sensitive to the exact definition of the shell radius.

The first three neighbor shells are well reproduced with respect to the experimental shape of Fig. 4 in Ref. 6. We express the partial projection on different pairs as $G_{\alpha\beta} = (1/N)\Sigma_{i\in\alpha, j\in\beta}^{r\leq R_c}\delta(r-r_{ij})-\rho_0$ to isolate their individual contribution. From Fig. 3 the As-Se pairs give the dominant contribution to the first shell. It is obvious that there exist homopolar bonds in our model. Se-Se pairs make a strong contribution in the range of the second shell, whereas As-As pairs have only a small effect. This is consistent with the picture inferred from the previous section of partial static factors. Our fourth peak near 7 Å did not agree with the experiment, indicating a deviation of pair correlation in the model. This may account for the incorrect position of the FSDP in the calculated $S(Q)$.

We focus on the local environment within the first-shell range of $G(r)$. The mean coordination number is 2.4 and the bond length from the first peak of $G(r)$ is 2.45 Å, agreeing with the experiment.[32] On average, As atoms have 3.01 neighbors and selenium 1.99 neighbors in the present model. All atoms in the first shell are distributed in the range 2.34–2.63 Å. The popular structure unit in the network of our model is the pyramidal AsX_3(X=As,Se) group. The As-X pyramid accounts for the first shell of $G(r)$ and the pyramidal length of X-X gives a contribution to the second shell of $G(r)$. The detailed coordination configuration of our model is given in Tables I and II for As and Se, respectively. A ball-and-stick image of a representative piece of our model is given in Fig. 4. About 96.5% of As is three-fold coordinated. While As coordination defects are rare, we found that the electronic states at the band edges derive from these coordination defects (to be discussed later). The pyramidal groups of As are not in perfect chemical order (e.g., exhibit homopolar bonds): only 46.5% of As is ideally chemically ordered. Also, only 60.5% of Se is two-fold coordinated. Of all the Se atoms 36.4% is in chemical order. The overall fraction of homopolar bonds is about 23%. The extended x-ray absorption fine structure experiment[10] led to an estimate that there were 10%–15% homopolar bonds in the evaporated As_2Se_3 films. However, the uncertainty in the estimation was also ±10%. Chang and Dove[13] have found that the experimental curve of the pair function can be fitted by the chemical ordered model and random bond model for As_2Se_3. They also found that to fit another chalcogenide film

TABLE I. Distribution of coordination configurations of As in model g-As_2Se_3.

Coordination number	Total number (in %)	Nearest-neighbor atoms	Number
2	1(1.2%)	1-Se and 1-As	1
3	83(96.5%)	3-Se	40
		2-Se and 1-As	30
		1-Se and 2-As	12
		3-As	1
4	2(2.3%)	4-Se	1
		2-Se and 2-As	1

As_2Te_3 the chemical order model required a larger thermal factor than the random bond model.

C. Intermediate-range order

Fundamentally IRO is a topic concerned with the connectivity among the structural building blocks. In c-As_2Se_3 the three Se atoms have two distinct positions: two Se atoms are elements of the As-Se spiral chains and the other Se bridges chains within layers. The repetition distance along the spiral axis is 4.3 Å which is missing from the amorphous structure[6] (see also Fig. 3 and Fig. 4). Another feature in the layer structure is a 12-member ring between neighbor spiral chains. In molecular As_4Se_6 all the Se atoms are at equivalent positions. A feature of this molecular structure is the four 6-member rings[12] which compose basically a compact connection of four pyramidal $AsSe_3$ by sharing Se atoms. The connection between pyramidal groups is very complicated in our model. Two types are most common: one is two pyramids XY_3 bridged by Se_n chain, the other is two pyramids XY_3 connecting directly to each other by sharing one bridging $Y(Y=\mathrm{As,Se})$. Table III gives a summary of the ring statistics for the n-member ring from $n=3$ to $n=12$. The four 6-member rings did not consist of molecular As_4Se_6.

Experiments[32] observe the FSDP near ~ 1.3 Å^{-1}. Some have proposed that it indicates an IRO in the range of 5.0 Å and others suspected that it arises from the molecular unit As_4Se_6. From our calculation it is difficult to say that the shoulder of $S(Q)$ near 1 Å^{-1} is assigned to an unambiguous correlation of IRO. In this connection, the calculated $S_{\alpha\beta}$ did not give a correct position of peak in the low-Q range but rather a deep valley of the $S_{\alpha\beta}$ near 1.3 Å^{-1}. It is also possible that the pair correlation in our model is not correct beyond the third-neighbor range. The other point is that the remainder term $R(QR_c)$ still has a strong contribution in this sensitive range. Because $R(QR_c)$ is only determined by the average density and the model size, not by the detailed correlation in the model, it is required to enlarge the truncation R_c or the size of model to push at least one more oscillation of j_1 out of the 1.3 Å^{-1} range for the sake of an unambiguous identification of the FSDP.

TABLE II. Distribution of coordination configurations of Se in model g-As_2Se_3.

Coordination number	Total number (in %)	Nearest-neighbor atoms	Number
1	26(20.2%)	1-As	21
		1-Se	5
2	78(60.5%)	2-As	47
		1-As and 1-Se	26
		2-Se	5
3	25(19.4%)	3-As	10
		2-As and 1-Se	13
		1-As and 2-Se	2

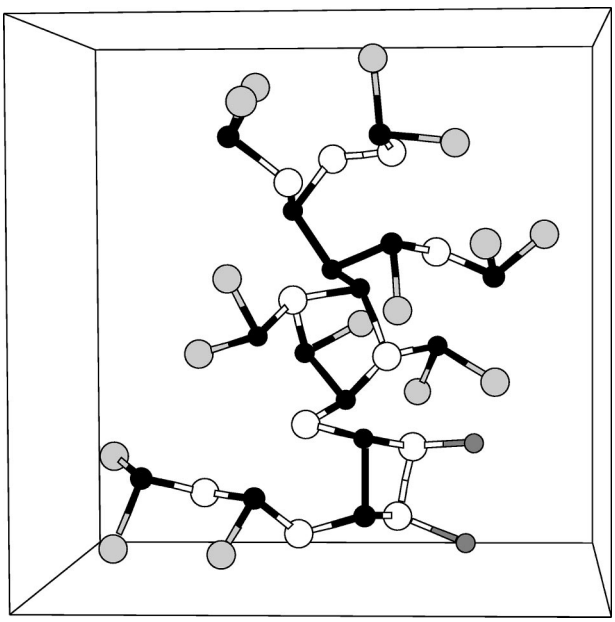

FIG. 4. A typical fragment of our model. Here, small black atoms are As, larger white are Se, and grey atoms are either species with additional bonds to other members of the network not shown in the image.

IV. DYNAMICAL PROPERTIES

The dynamical properties of our model are characterized by the vibrational density of states (VDOS). The features of localization in the vibration modes are analyzed by the inverse participation ratio (IPR). The computational methodology follows the previous study of g-$GeSe_2$ of our group.[28] We use the program XMOL (Ref. 33) to visualize the atomic motion to report the vibrational modes.

The calculated VDOS is compared with the experimental inelastic neutron scattering results[18] in Fig. 5. The overall agreement is rather good. The VDOS can be divided into two main bands. The low-energy band goes up to 20 meV. After a valley the high-energy band decays near 40 meV. Experiments determined that the lower band is nearly identical for the same average coordination number over a wide range composition in Se-As-Ge alloys.[18] It is proposed that those

TABLE III. Ring statistics. The number of n-member rings, $n=3$–12.

Ring size	3	4	5	6	7	8	9	10	11	12
Number of rings	2	3	11	4	5	5	2	3	2	6

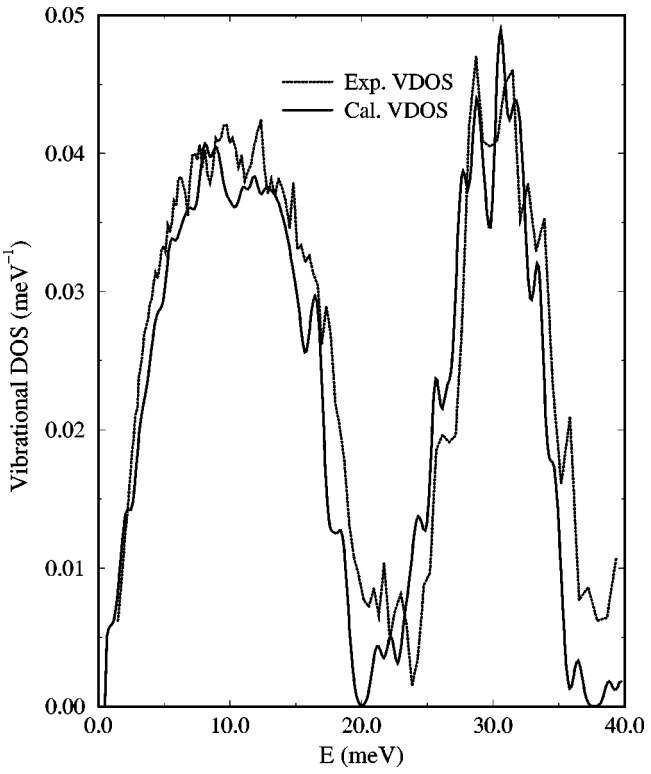

FIG. 5. Comparison between the calculated and experimental vibrational density of states for g-As_2Se_3.

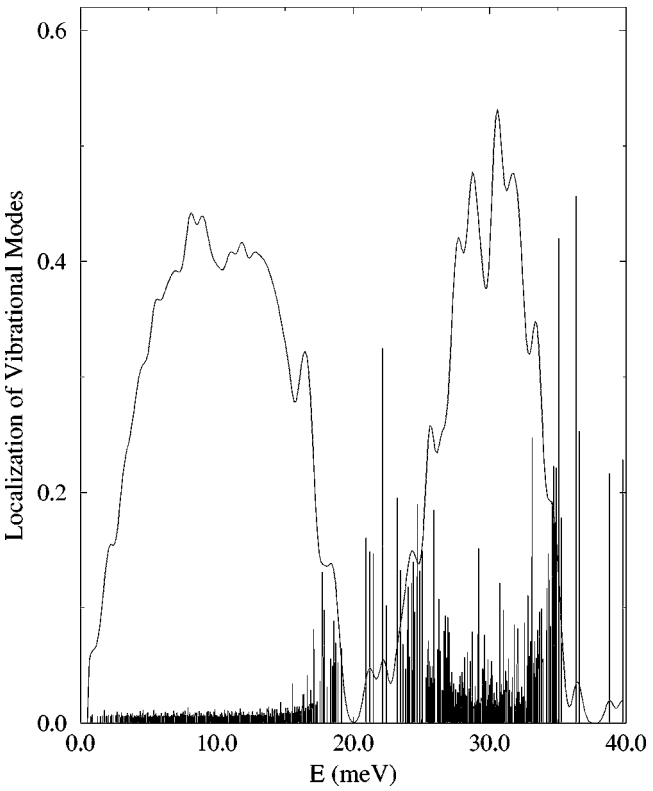

FIG. 6. Total inverse participation ratio (localization) of vibrational modes. The VDOS is plotted to guide the position of vibrational modes in model g-As_2Se_3, the intensity is enlarged by a factor.

modes in the low-energy band are sensitive only to connectivity rather than the short-range order in the glass as a VIR.[18] Our IPR analysis shows in Fig. 6 that the modes below 20 meV are rather extended over the network, giving a direct numerical support to the experimental conjecture. The localized modes appear at the edges of main bands. The same localization feature in the distribution of the vibrational modes is also observed in the vibration of g-$GeSe_2$.[28] The key structural unit in our model is XY_3 groups. However, because of the chemical disorder, about 23.1% of the X is occupied by Se. Using a molecular model, Lucovsky and Martin[15,16] have calculated a mode of 27.28 meV ($\sim$220 cm^{-1}) to be an antisymmetric stretching mode (γ_3) of $AsSe_3$ and the symmetric stretching mode (γ_1) is at 28.14 meV ($\sim$227 cm^{-1}). Ewen, Sik, and Owen[17] performed a valence force field calculation for the As-Se-Se-As chain which yields a value of 33.23 meV ($\sim$268 cm^{-1}) for the symmetric stretching frequency of the Se-Se bond. Lucovsky *et al.*[34] attributed the 29.76 meV ($\sim$240 cm^{-1}) vibration to As atoms having less than three Se neighbors. All these calculations were based on an isolated molecular model. However, because of the different forms XY_3 and complicated connection of Se chains, the localized vibrational modes have a rather broad distribution compared to the simple calculation on the chemically ordered cluster models as shown in Fig. 6. Both As and Se are involved in the local modes as indicated by Fig. 7. Analysis shows the local modes from 26.9 to 28.52 meV arise from three types of groups: single pyramidal XY_3, connected pyramids $(Y_2)X$-$X'(Y_2')$, and single bridging Se chain -As-Se-As-. By direct visual inspection it appears that the basic atomic vibrational mode of the three groups is antisymmetric stretching mode γ_3. The symmetric stretching mode γ_1 occurs at higher energy. In the γ_1 mode X moves opposite to three Y while in γ_3 there is one Y moving toward X. Above 28.52 meV long bridging -As-Se-Se-As- chain modes occur. Most of the local modes between 28.52 and 31 meV involve the single bridging Se chain or the connected two pyramidal XY_3. There are in this range combinations of γ_1 and γ_3 modes, which comply with the connection between the unit XY_3. Two five-member rings (4-Se and 1-As) contribute at 29.14 and 30 meV and one three-member ring (2-Se and 1-As) at 29.38 meV ($\sim$237 cm^{-1}). We mention that some have used the mode at 29.38 meV as an indicator of the layer structure in g-As_2Se_3.[11] After 31 meV single XY_3 recur until about 33.1 meV, and only one connected two pyramidal XY_3 is localized at 31.74 meV. Most of other local modes are the bridging Se chains. The localization on the higher edge of the high-energy band becomes more complicated. Long chains are involved. The most localized vibrations are on Se_n chains occurring always at the high-energy tail of the high-energy band.

V. ELECTRONIC STRUCTURE

The electronic density of states (EDOS) is calculated and analyzed by the inverse participation ratio.[28] Our EDOS is compared with the available experimental results[35] in Fig. 8. The agreement is impressive. The valence band of the EDOS consists of two main bands. The upper band is from 0 to about -6 eV below the top of the valence band or the highest occupied molecular orbital (HOMO) (we have shifted the

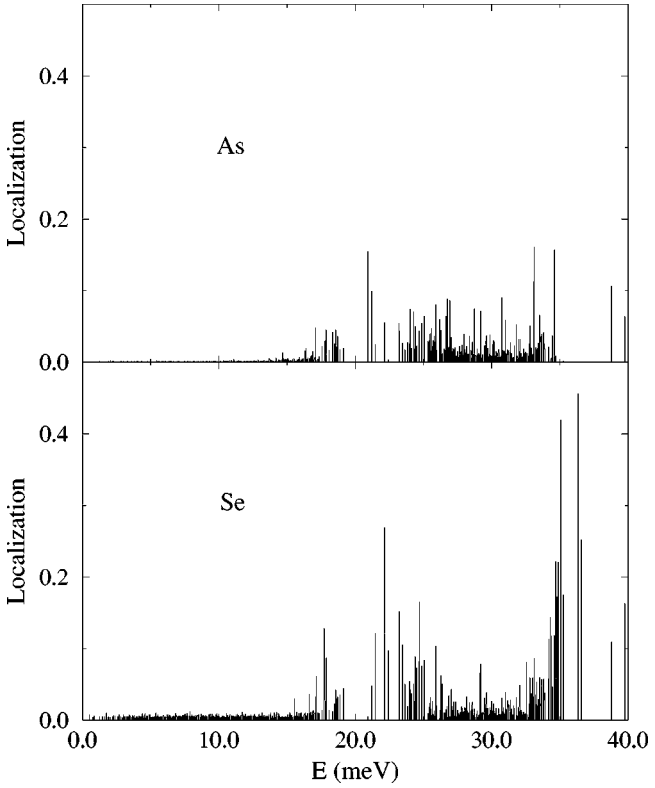

FIG. 7. Projected inverse participation ratio (localization) of vibrational modes on As and Se.

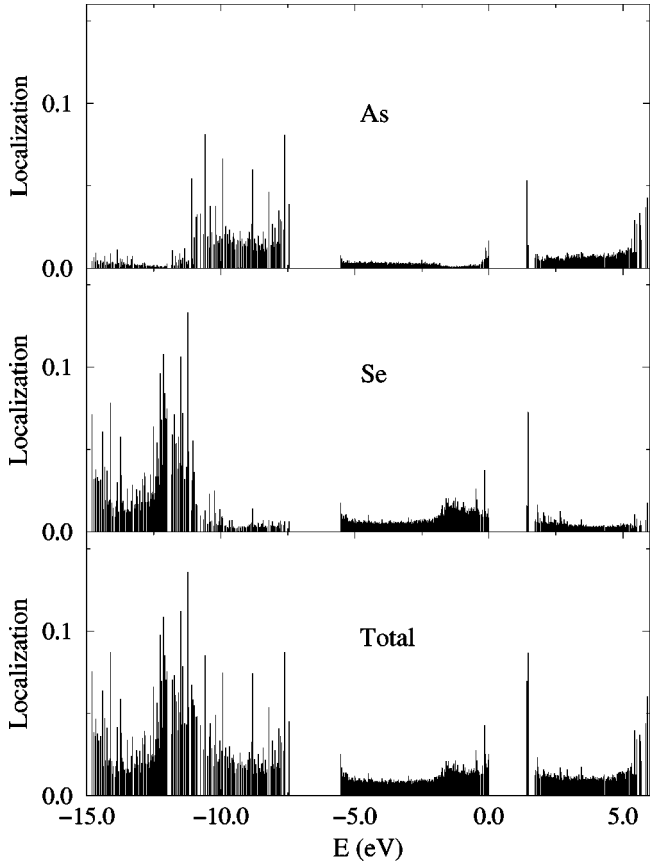

FIG. 9. Total and projected inverse participation ratio (localization) of electronic states for model g-As_2Se_3. The Fermi level lies between 0 and 2.0 eV.

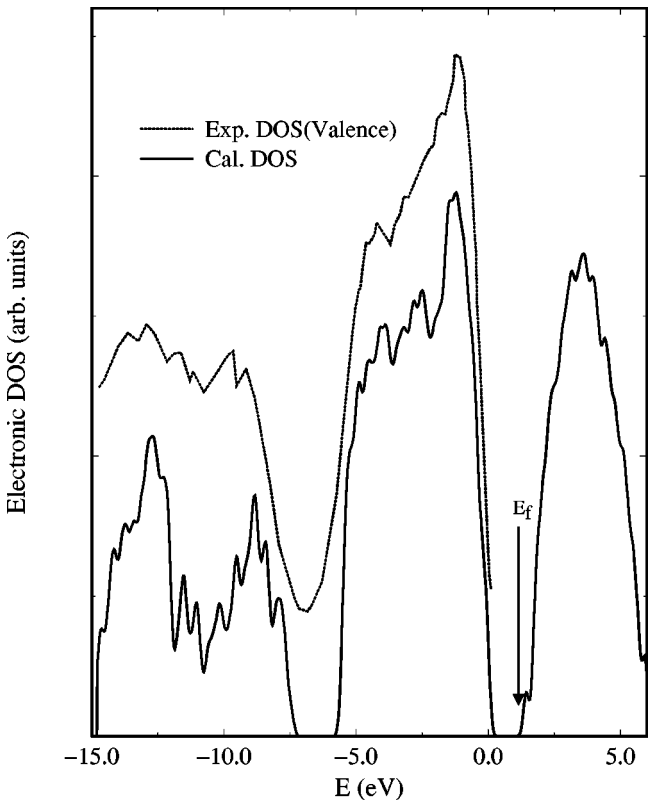

FIG. 8. Comparison between the calculated and experimental electronic density of states for g-As_2Se_3. The zero-energy reference is at the top valence state. The experiment provides only the valence band.

zero energy reference to the HOMO). The weaker lower band extends from about -7 eV to -15 eV below the HOMO. The upper band is attributed to the $4p$ electrons of As and Se while the lower band is from the more localized $4s$ electrons. Because of one more nuclear charge, the $4s$ electrons band of Se is below the corresponding $4s$ band of As. The upper band is a mixed type. Thus the localization is rather small except of at the band edge. These features can be seen clearly from the IPR in Fig 9.

Near the optical gap, there is a distinctive peak deriving mainly from Se atoms and As atoms which provides a smaller contribution to this peak region. The leading peak, in the range -2 to 0 eV, is attributed to the lone-pair band of Se,[35] which is similar to topmost valence band of Se.[22] Below the leading peak about 2 eV is the bonding band of $4p$ from both As and Se. One can observe that As is more involved in the bonding region than the leading region of the upper valence band. The As-Se bonds greatly reduce the splitting of the upper valence band compared to the pure Se. It is rather interesting that there are no band-gap states in our EDOS. However, the states near the band edge are well localized. We found all the localized edge states derive partly from the coordination defects of As. It is found that the HOMO is localized on the only one twofold coordinated As (see Table I) and the lowest unoccupied molecular orbital (LUMO) and the second LUMO are populated on the only two fourfold-coordinated As. The properties of states near the band edge are crucial to the optical and photostructural properties of g-As_2Se_3. It is well known that band-gap excitation or light-induced effects involves those states near the

band edge. The calculated gap between the HOMO and LUMO is 1.42 eV, which is very close to the experimental value[36] 1.74 eV.

VI. CONCLUSIONS

By use of first-principles MD simulations the properties of g-As_2Se_3 was studied using a 215-atom model. Our model gives good and uniform agreement with the experimental studies of the structure, dynamical, and the electronic properties. Although there is a fuzzy peak near 1.3 $Å^{-1}$ in the calculated $S(Q)$ which indicates a correlation beyond the third-nearest neighbors of at least 6.5 Å, we felt that a larger model is required to unambiguously manifest the FSDP feature near 1.3 $Å^{-1}$. The most popular local modes arise from the basic pyramidal XY_3 unit, the connected two pyramidal $(Y_2)X-X'(Y_2')$, and the bridging Se_n chain. Because As and Se have so much similarity in dynamical properties, all the possible modes mix in the similar frequency range. Compared to the similarity of dynamical properties of As and Se the electronic structure shows key distinctions between elements. The leading peak near the HOMO is from $4p$ nonbonding electrons of Se. The bonding $4p$ electrons of Se give the shoulder in the upper valence band after the leading peak with $4p$ electrons of As. Both $4s$ electrons of As and Se are localized in the weaker lower band. It is of interest that there are no gap states in the fundamental gap.

It is well known that the structure and properties of amorphous materials are sensitive to the method of preparation.[10] Similarly, different paths of MD simulation must give different models. Our work is limited in the sense that we can advance only one model in this paper because of the computational expense in forming such models. Still, because the model is relatively large (215 atoms) and also because there appears to be only a few basic types of ''building blocks'' in this glass, it is reasonable to take our model as representative of the glass. To make rigorous conclusions with unambiguous error bars concerning fracions of wrong bonds, for example, is difficult with this or similar calculations and one needs to understand this as a limitation of this type of approach.

ACKNOWLEDGMENTS

This work was supported in part by the National Science Foundation under Grant Nos. DMR 96-04921 and DMR 96-18789. We thank Professor Normand Mousseau and Professor Ron Cappelletti for helpful discussions.

[1] J.C. Phillips, J. Non-Cryst. Solids **43**, 37 (1981).
[2] M.F. Thorpe, J. Non-Cryst. Solids **57**, 355 (1983).
[3] H. Hisakuni and K. Tanaka, Science **270**, 974 (1995).
[4] V.V. Poborchii, A.V. Kolobov, and K. Tanaka, Appl. Phys. Lett. **74**, 215 (1999).
[5] K. Shimakawa, A. Kolobov, and S.R. Elliott, Adv. Phys. **44**, 475 (1995).
[6] A.L. Renninger and B.L. Averbach, Phys. Rev. B **8**, 1507 (1973).
[7] O. Uemura, Y. Sagara, D. Muno, and T. Satow, J. Non-Cryst. Solids **30**, 55 (1978).
[8] O. Luksha, V. Ivanitsky, and S. Kolinko, J. Non-Cryst. Solids **136**, 43 (1991).
[9] A.L. Renninger, M.D. Rechtin, and B.L. Averbach, J. Non-Cryst. Solids **16**, 1 (1974).
[10] R.J. Nemanich, G.A.N. Connell, T.M. Hayes, and R.A. Street, Phys. Rev. B **18**, 6900 (1978).
[11] P.C. Taylor, S.G. Bishop, and D.L. Mitchell, Phys. Rev. Lett. **27**, 417 (1971).
[12] J.P. De Neufville, S.C. Moss, and S.R. Ovshinsky, J. Non-Cryst. Solids **13**, 191 (1974).
[13] J. Chang and D.B. Dove, J. Non-Cryst. Solids **16**, 72 (1974).
[14] A.J. Leadbetter and A.T. Apling, J. Non-Cryst. Solids **15**, 250 (1974).
[15] G. Lucovsky, Phys. Rev. B **6**, 1480 (1972).
[16] G. Lucovsky and R.M. Martin, J. Non-Cryst. Solids **8-10**, 185 (1972).
[17] P. J. S. Ewen, M. J. Sik, and A. E. Owen, in *The Structure of Non-Crystalline Materials*, edited by P. H. Gaskell and E. A. Davis (Taylor & Francis, London, 1977), p. 231.
[18] B. Effey and R.L. Cappelletti, Phys. Rev. B **59**, 4119 (1999).
[19] W.A. Kamitakahara, R.L. Cappelletti, P. Boolchand, B. Halfpap, F. Gompf, D.A. Neumann, and H. Mutks, Phys. Rev. B **44**, 94 (1991).
[20] I. Chen, Phys. Rev. B **7**, 3672 (1973); **8**, 1440 (1973).
[21] M. Kastner, Phys. Rev. Lett. **28**, 355 (1972).
[22] M. Schlüter, J.D. Joannopoulos, and M.L. Cohen, Phys. Rev. Lett. **33**, 89 (1974).
[23] X. Zhang and D. A. Drabold, Phys. Rev. Lett. **83**, 5042 (1999).
[24] A.A. Demkov, J. Ortega, O.F. Sankey, and M. Grumbach, Phys. Rev. B **52**, 1618 (1995).
[25] O.F. Sankey and D.J. Niklewski, Phys. Rev. B **40**, 3979 (1989); O.F. Sankey, D.A. Drabold, and G.B. Adams, Bull. Am. Phys. Soc. **36**, 924 (1991).
[26] P. Stumm, D.A. Drabold, and P.A. Fedders, J. Appl. Phys. **81**, 1289 (1997).
[27] D.A. Drabold, P.A. Fedders, S. Klemm, and O.F. Sankey, Phys. Rev. Lett. **67**, 2179 (1991).
[28] M. Cobb, D.A. Drabold, and R.L. Cappelleti, Phys. Rev. B **54**, 12 162 (1996).
[29] P. Stumm and D.A. Drabold, Phys. Rev. Lett. **79**, 677 (1997).
[30] A.L. Renninger and B.L. Averbach, Acta Crystallogr., Sect. B: Struct. Crystallogr. Cryst. Chem. **29**, 1583 (1973).
[31] P.A. Doyle and P.S. Turner, Acta Crystallogr., Sect. A: Cryst. Phys., Diffr., Theor. Gen. Crystallogr. **24**, 390 (1968).
[32] Y. Sagara, O. Uemura, S. Okuyama, and T. Satow, Phys. Status Solidi A **31**, k33 (1975).
[33] Computer program XMOL, version 1.3.1, 1993, Minnesota Supercomputer Center, Inc., Minneapolis, MN 55415.
[34] G. Lucovsky, F. L. Galeener, R. H. Geils, and R. C. Keezer, in *The Structure of Non-Crystalline Materials*, edited by P. H. Gaskell and E. A. Davis (Taylor & Francis, London, 1977), p. 127.
[35] K.S. Liang, J. Non-Cryst. Solids **18**, 197 (1975).
[36] E.J. Felty, G. Lucovsky, and M.B. Myers, Solid State Commun. **5**, 555 (1967).